PAPER

Check for updates

A new approach for ultra-high adsorption of cationic methylene blue in a Zr-sulfonic-based metal–organic framework†

Thinh T. M. Bui, Linh T. Nguyen, Nha P. H. Pham, Cuong C. Tran, Loc T. Nguyen, Tien A. Nguyen, Hung N. Nguyen and My V. Nguyen [iD] *

A series of Zr-sulfonic-based metal–organic frameworks have been synthesized by the solvothermal method, namely VNU-17 and VNU-23. Particularly, VNU-17 and VNU-23 adopt the sulfonate group (SO_3^-) moieties densely packed within their structure, which can efficiently uptake MB^+ from wastewater. The maximum adsorption capacity for MB^+ onto VNU-23 is up to 1992 mg g^{-1} at pH = 7, which is more than five times that of activated carbon and possesses the highest value among all the reported MOF materials. In addition, VNU-23 retains the adsorption uptake of MB for at least five cycles. The adsorption isotherms and kinetic studies reveal that MB^+ dye adsorption onto VNU-23 fits a Langmuir isotherm and the pseudo second order kinetic model. Furthermore, the ultra-high adsorption capacity of VNU-23 for MB dye can be accounted for by the suitable pore/channel size together with electrostatic attraction and π–π interactions. These results indicate that VNU-23 can be utilized as a promising candidate for removing MB^+ from an aqueous medium.

1. Introduction

With the rapid development of industry and population growth, organic dyes have become crucial contaminants in water, which cause imbalance in ecosystems and affect human health.[1,2] Cationic dyes, such as methylene blue (MB), raise severe environmental concerns due to their various applications in dyeing cotton, wool, silk, and coloring paper.[3] Hence, removing organic dyes from wastewaters is extremely necessary before discharging them into the natural environment. There are many approaches to remove these pollutants, such as catalysis,[4–6] advanced oxidation processes,[7] flocculation,[8] membrane filtration,[9] and electrolysis.[10] Apart from these methods, adsorption has emerged as the most efficient technique to purge hazardous substances from wastewater due to its fleetness, low cost, high yield, insignificant dangerous by-products, and simplicity.[11–16] Different adsorbents have been utilized for the mentioned purpose, such as activated carbon,[17,18] metal oxide,[19] chitosan,[20] and carbon nanotube.[21] Nevertheless, there are several drawbacks to using these adsorbents such as slow adsorption kinetics, tricky generation, thermal and chemical instability, and low specific surface area. Finding a general strategy for

designing novel materials to improve the adsorption performance has been attracting much attention.

Metal–organic frameworks (MOFs) are crystalline and porous materials, which adopt permanent porosity, the modular essence of constitution and synthesis. Compared with other adsorbents, MOFs have many dominant features, such as high ordered structure, good thermal and chemical stability, low density, and large specific surface area. Consequently, MOFs can be added to an assorted arrangement of functional groups and guest molecules. It allows MOFs to be extraordinary scaffolds in various utilizations.[22] As expected, MOFs have been employed as efficient adsorption materials for the removal of dyes. Besides, increased stability in water and facile modification of the ligand are the unique properties of MOFs in the adsorption of pollutants. By adding positive and negative charge groups into MOFs, the possibility of removal of contaminants from wastewater has been significantly enhanced through the electrostatic interaction mechanism.[23–27]

However, only a few MOFs display a high removal level of pollutants, leading to poor application in the treatment of practical wastewater.[23,28] Moreover, there is no specific strategy in the design and synthesis of MOFs that can create an ultra-high adsorption capacity for organic dyes. With this in mind, we expect that introducing dense charge carrier moieties such as sulfonate groups ($-SO_3^-$) inside the structure of MOFs to enhance the interaction between MB^+ cations and SO_3^- groups *via* electrostatic attraction can lead to an excellent adsorption capacity for MB^+.

Faculty of Chemistry, Ho Chi Minh City University of Education, Ho Chi Minh City 700000, Vietnam. E-mail: mynv@hcmue.edu.vn

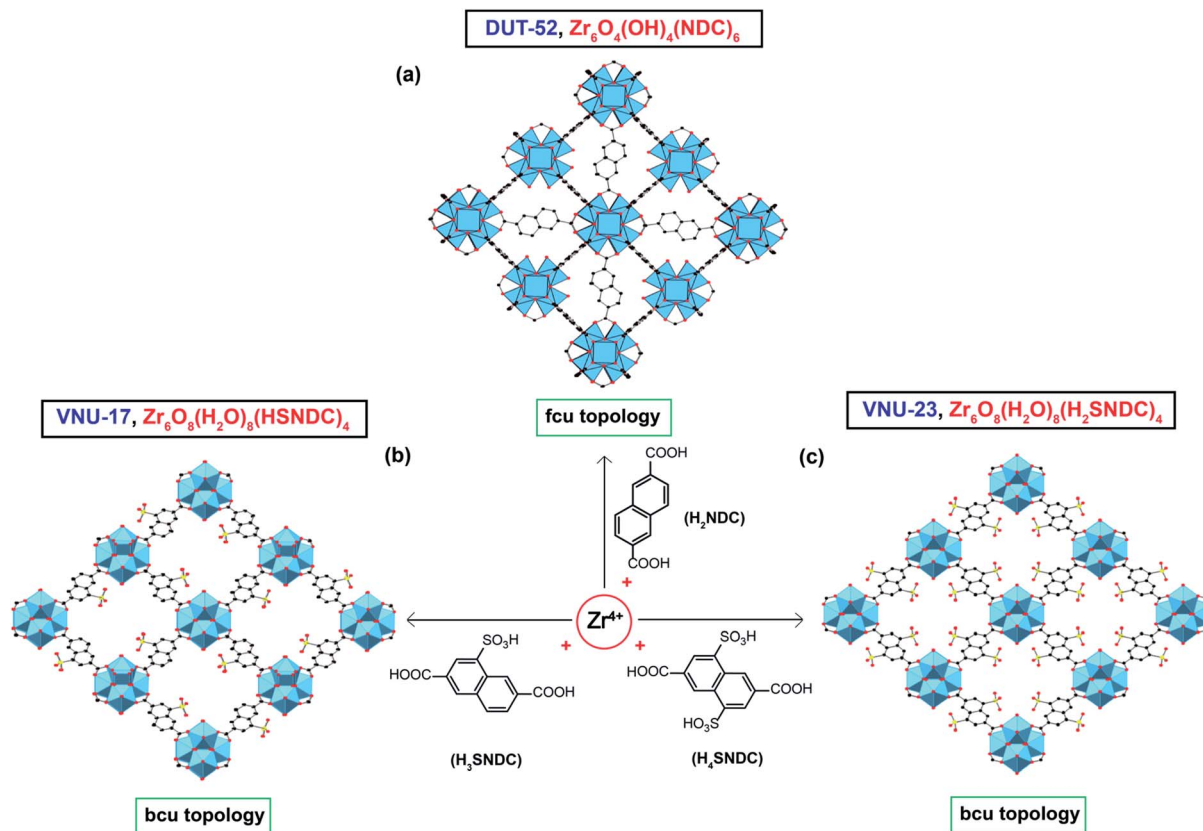**Fig. 1** The architecture of DUT-52 is constructed from 12-connected $Zr_6O_4(OH)_8(NDC)_6$ to form a structure adopting the **fcu** topology (a), which is depicted from a CCDC number of 937877.[31] The design of VNU-17, $Zr_6O_8(H_2O)_8(HSNDC)_4$, and VNU-23, $Zr_6O_8(H_2O)_8(H_2SNDC)_4$, is depicted (b and c) with 8-connected **bcu** topology, which is constructed from the cif information of previously reported VNU-17 and VNU-23 with the CCDC number of 1540864 and 1585550, respectively.[29,30] Atom colors: Zr, blue polyhedra; C, black; O, red; S, yellow. All H atoms are omitted for clarity.

With all of this taken into consideration, we developed an approach for synthesizing a series of Zr-sulfonic-based MOFs, constructed from $Zr_6O_8(H_2O)_8(COO)_8$ cluster and sulfonic-rich linkers such as 4-sulfonaphthalene-2,6-dicarboxylic acid (H_3SNDC) and 4,8-disulfonaphthalene-2,6-dicarboxylic acid (H_4SNDC), namely VNU-17 and VNU-23. As in our previous studies,[29,30] VNU-17 and VNU-23 possessed the **bcu** topology (Fig. 1b, c), highlighted by suitable pore windows for introducing MB *via* electrostatic attraction (Fig. S1†). As expected, VNU-23 exhibited a maximum adsorption capacity (q_m) for MB of about 1992 mg g^{-1} at pH = 7, with adsorption uptake maintained without any appreciable loss for at least five cycles (Fig. 6). These findings demonstrated the adsorption performance for MB for systematically fine-tuning such materials for use as absorbents in practical conditions.

2. Experimental

Synthesis of 4-sulfonaphthalene-2,6-dicarboxylic acid (H_3SNDC) linker

A mixture of 2,6-naphthalenedicarboxylic acid (1 g, 4.63 mmol) and 10 mL of oleum (SO_3 in concentrated H_2SO_4, 10 wt%) was added to a 100 mL glass flask and then stirred at 130 °C for 1

day. The solution was cooled to room temperature and the product was dissolved in 100 mL of distilled water, filtered and precipitated by 50 mL of concentrated HCl (37 wt%). Next, the solid was filtered, washed with 100 mL of concentrated HCl and dried at 80 °C under vacuum for 1 day to give a pure linker at 80% yield. ^{1}H-NMR (DMSO-d_6, 500 Hz): δ = 9.51 (s, 1H); 8.52 (s, 1H); 8.48 (s, 1H); 8.10 (d, 1H, J = 0.02 ppm); and 7.99 ppm (d, 1H, J = 0.02 ppm) (Fig. S2†).

Synthesis of 4,8-disulfonaphthalene-2,6-dicarboxylic acid (H_4SNDC) linker

A mixture of 2,6-naphthalenedicarboxylic acid (1 g, 4.63 mmol) and 10 mL of fuming sulfuric acid was introduced into a 100 mL glass flask and continuously stirred and refluxed at 150 °C for 1 day. Next, fresh fuming sulfuric acid (6 mL) was added and then stirred and refluxed at 170 °C for 2 days. The reaction mixture was then cooled to room temperature, and the mixture was slowly dropped into 200 mL of distilled water, filtered and precipitated by 100 mL of concentrated HCl (37 wt%). Finally, the solid was filtered, washed with 200 mL of concentrated HCl and dried under vacuum at 80 °C for 1 day to yield a gray-white powder. ^{1}H-NMR (DMSO-d_6, 500 Hz): δ = 9.52 (s, 2H); 8.47 (s, 2H) (Fig. S2†).

Synthesis of VNU-17

A mixture containing $ZrOCl_2 \cdot 8H_2O$ (0.052 g, 0.162 mmol), H_3SNDC linker (0.054 g, 0.183 mmol), formic acid (1.3 mL), and DMF (8 mL) was heated at 120 °C for 2 days. The mixture was then cooled to room temperature. The solid was centrifugated and washed with DMF for 3 days (6 mL per day). The material was then immersed in a $MeOH/H_2O$ (v/v = 4/1) solution of H_2SO_4 0.3 M for 3 days (0.3 M H_2SO_4, 5 times per day). Next, the material was washed to pH = 5 with an excess amount of methanol/H_2O (v/v = 4/1). The solid was exchanged with MeOH for 2 days (5 × 5 mL per day), centrifugated, and activated under vacuum at 80 °C for 1 day to yield a pure acidified VNU-17 (82% yield, based on Zr^{4+}).

Synthesis of VNU-23

$ZrOCl_2 \cdot 8H_2O$ (0.0393 g, 0.122 mmol), H_4SNDC linker (0.0496 g, 0.132 mmol), formic acid (1.5 mL), and DMF (6 mL) were ultrasonically dissolved for 10 min in a 20 mL Pyrex vial. The mixture was then heated at 120 °C for 2 days. After cooling down to room temperature, the gray-white powder was collected by centrifugation.

Subsequently, the product was washed with DMF for 3 days (6 mL per day). Next, this material was soaked in a methanol/H_2O (v/v = 4/1) solution of H_2SO_4 for 2 days (0.3 M H_2SO_4, 5 times per day). The sample was washed to pH = 5 with an excess amount of methanol/H_2O (v/v = 4/1). Finally, this material was exchanged with MeOH for 2 days (5 × 5 mL per day), centrifugated, dried and activated under vacuum at 80 °C for 1 day to yield an acidified VNU-23 (70% yield, based on Zr^{4+}).

Batch adsorption experiment

The MB adsorption studies were carried out at room temperature under a constant stirring rate (500 rpm). An adsorbent dosage of VNU-23 of 5–30 mg was introduced to the initial concentration of MB of 20 mg L^{-1}. To study the effect of initial pH on the adsorption behaviour, 500 mg L^{-1} of MB was chosen as the initial concentration with the dosage of VNU-23 of about 0.25 g L^{-1} after stirring for 24 h. The initial pH (3–10) of MB was adjusted by the addition of 0.01 M NaOH and 0.01 M HCl solutions and recorded using a pH meter. The spectrum of MB solutions was analysed on a UV-vis spectrophotometer at a maximum wavelength of 663 to 664 nm. The concentration of MB was determined by using a calibration curve made from the standard solutions (Fig. S3 and S4†).

The adsorption capacity (mg g^{-1}) at equilibrium (q_e) and time t (q_t) and removal percentage ($R\%$) in the case of MB were calculated by using the following equations:

$$q_0 = \frac{(C_0 - C_e)}{m} \times V \qquad (1)$$

$$q_t = \frac{(C_0 - C_t)}{m} \times V \qquad (2)$$

$$R\% = \frac{(C_0 - C_t)}{C_0} \times 100 \qquad (3)$$

where C_0, C_t and C_e are the concentration of MB at initial, t and equilibrium time, respectively. V (mL) is the volume of the solution and m (mg) symbolizes the adsorbent mass.

To investigate the adsorption isotherms, 25 mg of VNU-23 was introduced to 100 mL of the MB solution (100–1600 mg L^{-1}) at pH = 7. The MB concentrations remaining in the supernatant solution after 24 h were measured.

Reusability

To study the reusability of the materials, a series of adsorption–desorption cycles were conducted. After the complete adsorption of MB at the specific conditions, the materials were centrifuged and then immersed and stirred in ethanol at pH = 3 as an effective desorption medium. Subsequently, the materials were dried under vacuum at 80 °C for 24 h, and then tested for the next adsorption experiment.

3. Results and discussion

Characterization of Zr-sulfonic-based MOF

As in previous reports,[29,30] VNU-17 and VNU-23 are successfully synthesized from a mixture containing $ZrOCl_2 \cdot 8H_2O$ salt and H_3SNDC for VNU-17 or H_4SNDC for VNU-23 in N,N-dimethylformamide (DMF) in the presence of formic acid as a modulator and heating at 120 °C for 1 day. To gain insight into the adsorption ability of these materials, we recall the structure of VNU-17 and VNU-23. They crystallize in the tetragonal space group, $I4/m$, with the unit cell of $a = b = 17.75$ and $c = 22.48$ Å. Particularly, VNU-17 and VNU-23 are iso-reticular, generated by 8-connected $Zr_6O_8(H_2O)_8(-CO_2)_8$, combined by $SNDC^{3-}$ and $SNDC^{4-}$ linker, respectively (Fig. 1b and c). This leads to a 3D structure based on **bcu** topology, different from that of DUT-52 (Fig. 1a).[31] Interestingly, VNU-17 and VNU-23 possess the dense SO_3^- groups within the framework, suitable for the adsorption of MB^+ *via* electrostatic attraction. Meanwhile, these groups exhibit a repulsive interaction towards a negative moiety like methyl orange (MO^-) (see Fig. 2b). The pure phases of the as-synthesized DUT-52, VNU-17 and VNU-23 are further evidenced by powder X-ray diffraction (PXRD) analyses (Fig. 2a), which are in good agreement with the previous works.[29,30] Additionally, to generate a perfect adsorption space within the
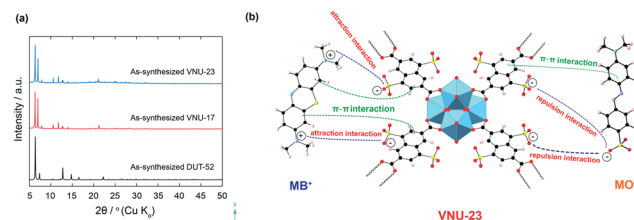
Fig. 2 Powder X-ray diffraction analysis of as-synthesized VNU-17 (red) and as-synthesized VNU-23 (blue) in comparison with as-synthesized DUT-52 (black) (a); the plausible adsorption mechanism of MB^+ and MO^- on VNU-23 (b). Herein, the structure of VNU-23 is illustrated from the cif information with the CCDC number of 1585550.[30] Atom colors: $Zr_6O_8(H_2O)_8$ cluster, blue polyhedra; C, black; O, red; N, blue; S, yellow; H, gray.

structure, these materials are immersed in H_2SO_4 (0.3 M) to remove dimethylammonium ions, which appears by the decomposition of DMF solvent in the synthetic process, and washed with an excess amount of the solvents to pH = 5. Also, Fourier transform infrared (FT-IR) and thermogravimetric analysis (TGA) are conducted, which confirm the presence of the sulfonate groups by the broad peaks at 1178 and 1190 cm^{-1} (Fig. S6†), and reveal the thermal stability of the materials up to 450 °C (Fig. S12†). Subsequently, we demonstrate that the chemical stability of the Zr-sulfonic-based MOFs in water is retained after 30 days, as evidenced by PXRD analysis (Fig. S8†). It is noted that the sulfonic-based MOFs lose the long-range structural order upon activation.[29,30] This is also in line with the N$_2$ adsorption analysis for the VNU-23 material (Fig. S14†); the BET surface area of the activated VNU-23 is lower than the theoretically predicted value. This phenomenon can be attributed to the flexibility of the SO$_3$H group after recovery, affecting the structural order of the materials.[32,33] However, the crystallinity is fully restored after immersing in water (Fig. S9†). The presence of MB molecules within VNU-23 is also confirmed by TGA analysis (Fig. S13†). Accordingly, the thermal gravimetric

curves indicate a weight loss of about 5 wt% from room temperature to 300 °C, which is attributed to the loss of coordinated water, followed by a steep drop from 300 to 600 °C. This steep drop is assigned to the loss of MB molecules and framework decomposition (Fig. S13†).

In order to inspect the effect of the number of SO$_3$H groups within the MOF on the MB adsorption capacity, a series of specific experiments are conducted. In detail, 10 mg each of DUT-52, VNU-17 and VNU-23 is introduced into 15 mL of MB (200–1000 mg L^{-1}) at an initial pH range of 4 to 5. Fig. 3a reveals that the adsorption capacities for MB (1000 mg L^{-1}) on DUT-52, VNU-17 and VNU-23 are 20.140, 314.75 and 1290.5 mg g^{-1}, respectively. The increase in the adsorption capacity upon raising the number of SO$_3$H groups within VNU-17 and VNU-23 can be attributed to the rise in the attraction forces between the highly negatively charged SO$_3^-$ moieties in the MOF and the positively charged MB molecules. In contrast, DUT-52 exhibits a very poor adsorption capacity for MB due to the absence of the SO$_3$H groups within the structure. Interestingly, we illustrate that the SO$_3^-$ moieties of VNU-23 can strongly attract the MB$^+$ ions and repulse the MO$^-$ ions as evidenced by the UV-vis
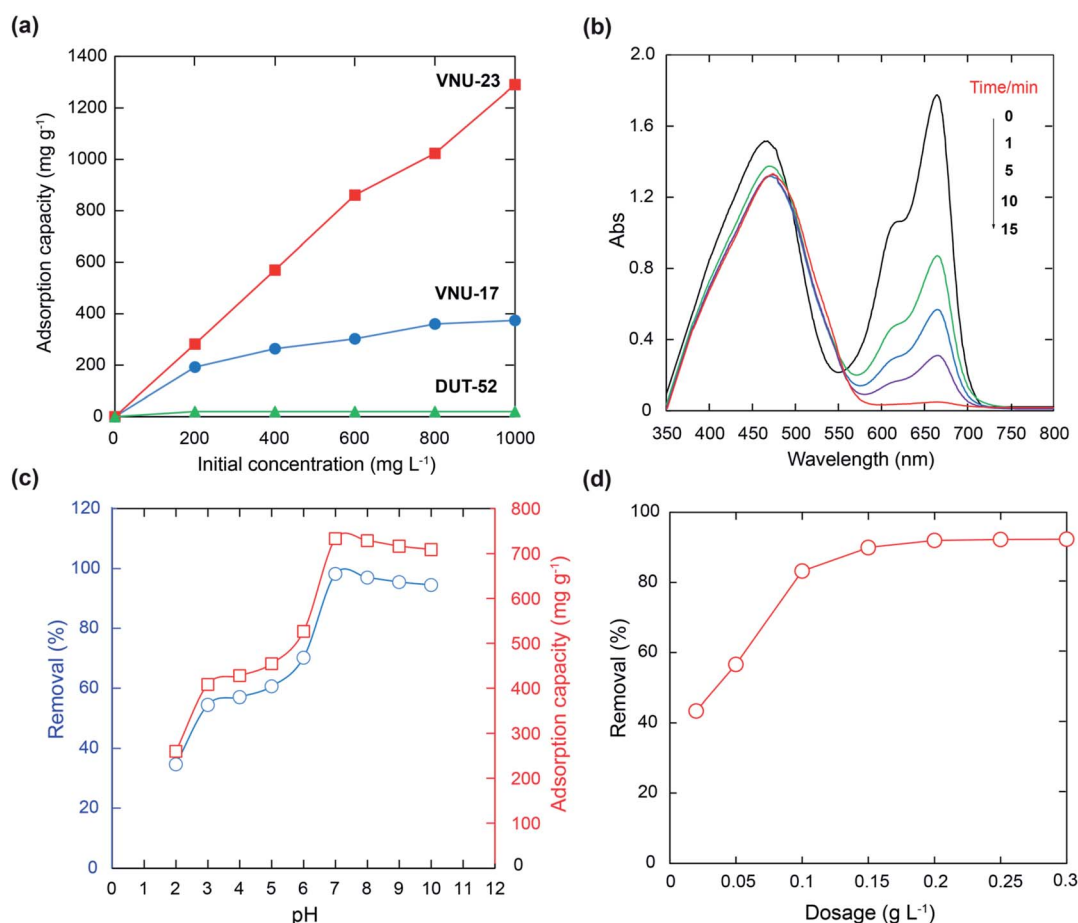
Fig. 3 Effect of the number of SO$_3$H groups within the structures of DUT-52, VNU-17 and VNU-23 on the adsorption capacity of MB [m = 10 mg, V_{MB} = 15 mL, t = 4 h, pH = 4–5] (a); the adsorption property of VNU-23 in a mixture of MB and MO [m = 10 mg, $C_{0(MB)}$ = 10 mg L^{-1}, $C_{0(MO)}$ = 20 mg L^{-1}, $V_{mixture}$ = 20 mL, t = 0–15 min] (b); effect of pH medium on the adsorption capacity and removal efficiency of MB on VNU-23 [m = 10 mg, C_0 = 500 mg L^{-1}, V_{MB} = 15 mL, t = 24 h] (c); effect of VNU-23 dosage on removal efficiency of MB [m = 2–30 mg, C_0 = 20 mg L^{-1}, V_{MB} = 100 mL, pH = 7, t = 24 h] (d).

spectrum (Fig. 3b). Specifically, the maximum peak at 464 nm of MO is significantly unchanged after 5 min, while the maximum peak at 664 nm of MB has almost disappeared after stirring for 15 min (Fig. 3b). Based on these data, VNU-23 is chosen for the following adsorption experiments in this main paper. In addition, as a full comparison and evaluation on the effect of the number of SO$_3$H groups, the kinetic studies, adsorption isotherm models, and reusability of VNU-17 are presented in Section S9.†

Effect of pH

Fig. 3c shows that the adsorption capacity and the removal efficiency of MB are raised with the increase in the pH value from 3 to 7. This behaviour can be accounted for by the increasing pH (3 to 7) of the MB solution leading to an increase in the magnitude of the negative charges on the surface of VNU-23, which in turn raises the electrostatic interaction between the SO$_3^-$ groups inside the MOF and MB$^+$. However, the removal and the adsorption capacity are reduced at a pH range from 8 to 10. This can be explained by the high competition between OH$^-$ ions and SO$_3^-$ components with MB$^+$ at a pH > 7, resulting in a decreased tendency of MB adsorption on VNU-23. Thus, the optimal pH of 7 is selected for the subsequent studies.

Effect of adsorbent dose

The effect of adsorbent dose on the adsorption of MB on VNU-23 is given in Fig. 3d. The removal efficiency rises with increasing adsorbent dose and reaches 93% with a dosage of 0.2 g L^{-1}. This result indicates that other active sites become available on raising the adsorbent dose, allowing more adsorbate ions to adhere to it.

Adsorption isotherm models

To study the essence of the merge between VNU-23 and MB, the Langmuir, Freundlich, Temkin, and Dubinin–Radushkevich isotherm models have been employed for the interacting liquid–solid phase.

The linear forms of the Langmuir and Freundlich models are displayed by eqn (4) and (5).[34]

$$\frac{C_e}{q_e} = \frac{1}{K_L q_m} + \frac{C_e}{q_m} \tag{4}$$

$$\log q_e = \log K_F + \frac{1}{n} \log C_e \tag{5}$$

where q_e and C_e are the MB removal amount and MB concentration at equilibrium, respectively, K_L is the Langmuir constant, q_m is the theoretical maximum capacity of MB adsorption, and K_F and n are the Freundlich constants.

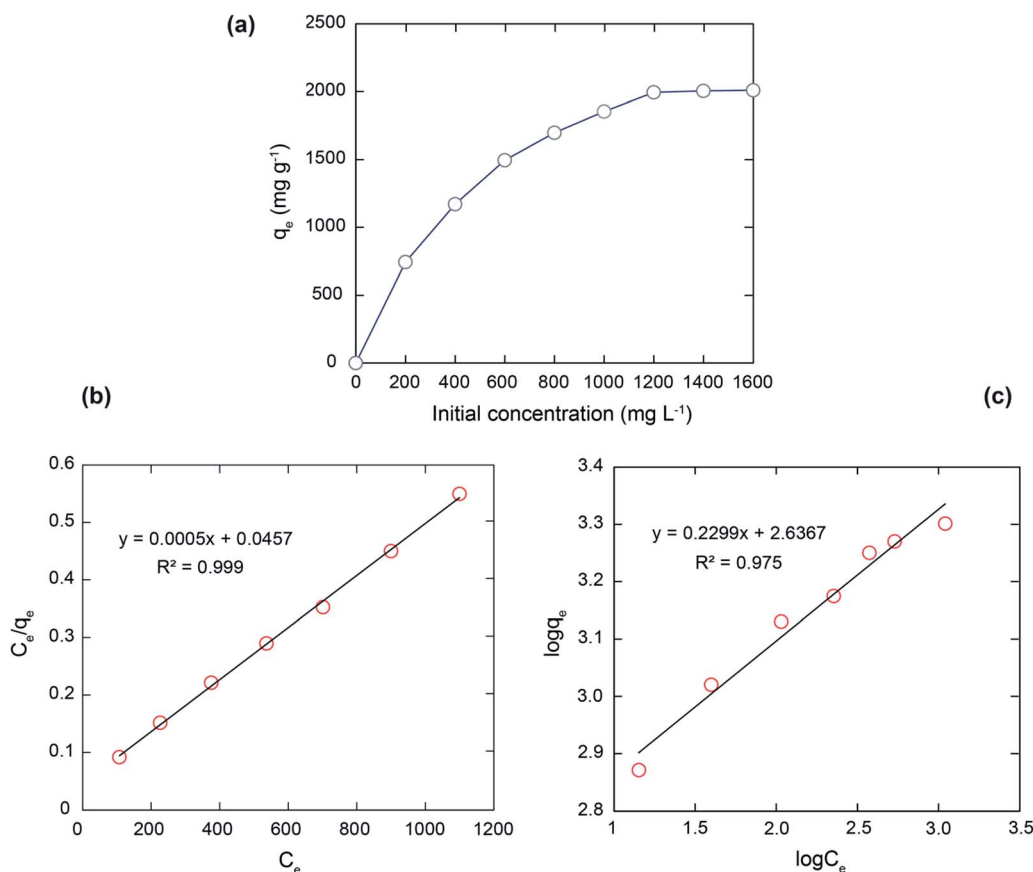**Fig. 4** Effect of initial concentration on the adsorption capacity of MB onto VNU-23 [$m = 20$ mg, $V_{MB} = 100$ mL, $C_0 = 200$–1600 mg L^{-1}, pH = 7, $t = 24$ h] (a). Data fitting with the adsorption isotherm models: Langmuir (b) and Freundlich (c).

Table 1 The parameters calculated from isotherm models for the adsorption of MB over VNU-23

Isotherms	Paramaters	Value
Langmuir	q_m (mg g^{-1})	**2000**
	K_L (L mg^{-1})	0.011
	R^2	**0.999**
Freundlich	$1/n$	0.230
	K_F (mg g^{-1} (L g^{-1})$^{1/n}$)	433.2
	R^2	**0.975**
Temkin	b	7.805
	k_T (L mg^{-1})	0.558
	R^2	**0.967**
DR	C (mol^2 J^2)	3×10^{-5}
	k_{DR} (mg g^{-1})	1623.6
	R^2	**0.755**

The Temkin model is also employed by eqn (6),

$$q_e = \frac{RT}{b} \ln(k_T C_e) \tag{6}$$

where R is the gas constant, b and k_T are the constant of adsorption heat and the constant of Temkin, respectively, and T is the adsorption temperature.

Furthermore, the isotherm of Dubinin–Radushkevich (DR) is investigated by eqn (7),

$$\ln q_e = \ln k_{DR} - C\varepsilon^2 \tag{7}$$

where ε is a constant, k_{DR} and C are the constant of DR isotherm and the adsorption energy per adsorbent molecule, respectively.

Fig. 4b, c and S19† reveal the linear plots of the Langmuir, Freundlich, Temkin and DR isotherms for the adsorption of MB on VNU-23, respectively. The model parameters, acquired by using the models to the experimental data, are also given in Table 1.

As given in Table 1, the equilibrium data are fitted better by the Langmuir model ($R^2 = 0.999$) than by the Freundlich model ($R^2 = 0.975$), Temkin model ($R^2 = 0.967$) and DR model ($R^2 = 0.755$) for the adsorption of MB onto VNU-23, suggesting that only a layer of the MB molecules is formed at the adsorption sites of the adsorbent. Hence, it can be supposed that the monolayer Langmuir adsorption isotherm is the corresponding model to describe MB adsorption onto VNU-23. It is noteworthy that the theoretical value of q_m (2000 mg g^{-1}) determined from the Langmuir model is much close to the experimental value (1992 mg g^{-1}, see Fig. 4a).

Also, the separation factor R_L, which is a vital parameter derived from the Langmuir model, is considered a credible magnitude for evaluating the adsorption favourability, where C_0 is the initial MB concentration and K_L is the Langmuir constant.

$$R_L = \frac{1}{1 + K_L C_0} \tag{8}$$

It is noted that the R_L value is found to be less than 1 and greater than zero, which can indicate the strong interactions
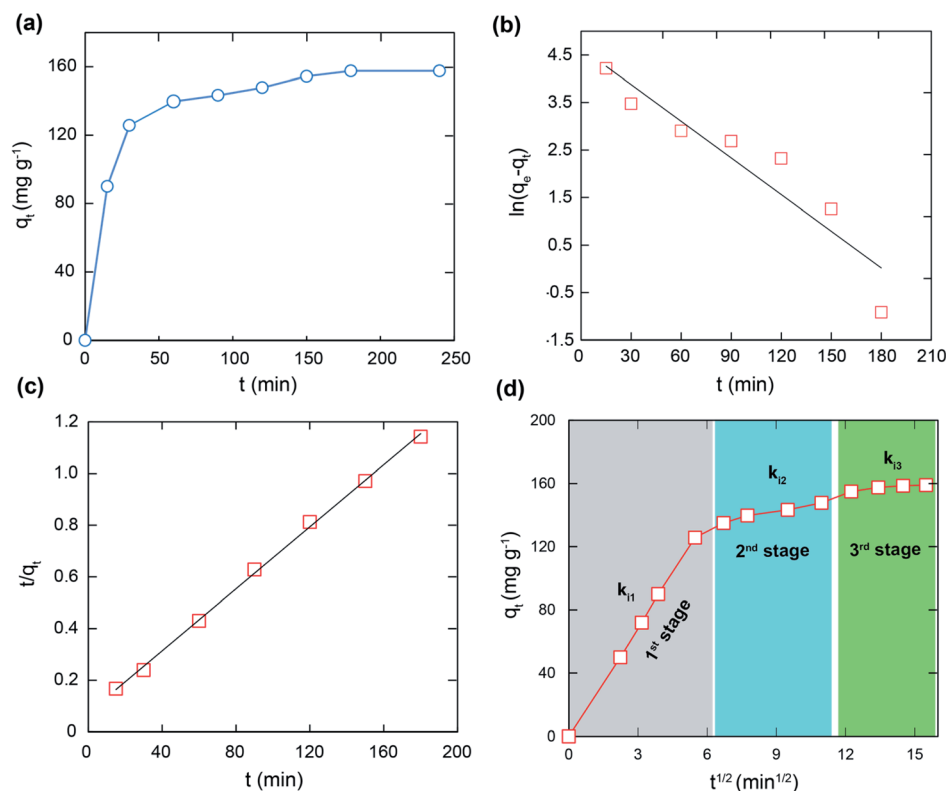
Fig. 5 The kinetic curve for the adsorption of MB on VNU-23 [m = 5 mg, V_{MB} = 20 mL, C_0 = 50 mg L^{-1}, pH = 7] (a). Data fitting with the adsorption models: pseudo first order (b), pseudo second order (c) and intra-particle diffusion model (d).

Table 2 Pseudo first order and second order model parameters for the adsorption of MB onto VNU-23

Kinetic models	Paramaters	Value
	$q_{e,exp}$ (mg g^{-1})	**159.8**
Pseudo first order	$q_{e,cal}$ (mg g^{-1})	**104.3**
	k_f (min^{-1})	0.026
	R^2	**0.882**
Pseudo second order	$q_{e,cal}$ (mg g^{-1})	**166.7**
	k_s (10^{-4}) (g mg^{-1} min^{-1})	4.912
	R^2	**0.999**

between the active sites of SO$_3^-$ and MB$^+$ ions. Also, the $1/n$ value obtained from the Freundlich model indicates the favourable process of MB over VNU-23.

Adsorption kinetics

To investigate the rate of adsorption mechanism of MB on VNU-23, studies on the kinetics of adsorption are conducted by the pseudo first order and pseudo second order models. The types of these models are determined by eqn (9) and (10), respectively. In addition, the intra-particle diffusion model is utilized for evaluating the MB adsorption ability onto VNU-23, exhibited by eqn (11).

$$\ln(q_e - q_t) = \ln q_e - k_f t \tag{9}$$

$$\frac{t}{q_t} = \frac{1}{k_s q_e^2} + \frac{t}{q_e} \tag{10}$$

$$q_t = k_i t^{1/2} + c \tag{11}$$

where q_t and q_e are the MB uptake amounts at t and equilibrium, respectively, k_f and k_s are the rate constants of pseudo first and second order, respectively, k_i is the rate constant of the intra-particle diffusion, and c is the constant exhibiting the thickness of the boundary layer.

The kinetic models and parameters are shown in Fig. 5 and Table 2. It is noted that the experimental value best fits the pseudo second order ($R^2 = 0.999$) than the pseudo first order ($R^2 = 0.882$). Significantly, the pseudo second order has a higher affinity between the experimental and calculated adsorption capacities. In fact, the pseudo second order is considered as the adsorption process controlled by the rate-limiting stage of

Table 3 Intra-particle diffusion model parameters for the adsorption of MB onto VNU-23

Intra-particle diffusion	Paramaters	Value
First stage	k_{i1}	23.15
	R^2	0.999
Second stage	k_{i2}	2.492
	R^2	0.987
Third stage	k_{i3}	1.883
	R^2	0.939

chemical adsorption, including the electron transfer and electron sharing process.[35,36]

Furthermore, the obtained results in Fig. 5d indicate that the adsorption is achieved through three stages.[37–39] In detail, the rate constant values (k_i) in Table 3 of the intra-particle diffusion process point out that $k_{i1} > k_{i2} > k_{i3}$ can be attributed to the change in the MB diffusion rate during three stages.
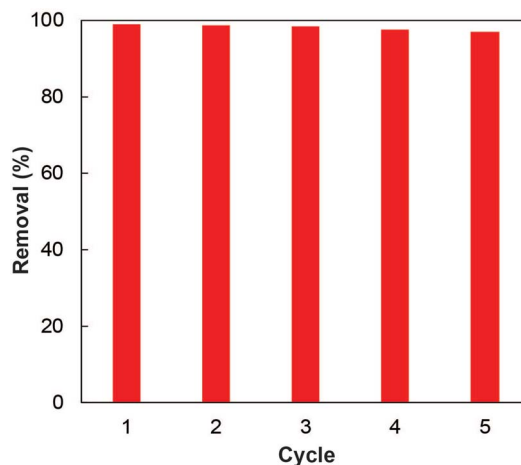
The first stage is fast and assigned to the boundary layer formed on the external surface of the VNU-23 framework, while the second stage is slower and can be ascribed to the entrance of the MB molecules into the internal surface. Finally, in the third stage, the MB molecules diffuse slowly into the pores and interact with the active sites of VNU-23 till the equilibrium is reached. Although the last stage is slow, it is not the controlling stage of the adsorption process, as the straight line does not pass through the origin.

Reusability

The reusability of VNU-23 has been studied through five cycles for MB removal. The adsorption uptake of MB onto VNU-23 is indicated in Fig. 6. A removal efficiency of 97% is retained after five cycles. It is worth mentioning that VNU-23 is easily reused after all the cycles of the adsorption process without loss of initial weight.

Furthermore, the achievable regeneration of VNU-23 is evidenced by the FT-IR spectra and PXRD analysis in Section S10.† After the adsorption of MB, the characteristic vibrations of MB are found in MB⊂VNU-23 (see Fig. S7†). However, after immersing in ethanol, these signals disappear, as shown in Fig. S21.† Also, a high degree of correspondence in the PXRD patterns is observed for the VNU-23 samples before and after the desorption of MB (Fig. S20†). These represent the ability to utilize VNU-23 as a potential and highly effective reusable candidate for practical applications in the removal of organic dyes from an aqueous environment.

A comparison of the maximum adsorption capacity (q_m) of VNU-23 with that of other reported adsorbents is represented in Table 4. It is seen that VNU-23 exhibits the highest adsorption

Fig. 6 The reusability of VNU-23 in the adsorption process of MB.

Table 4 The maximum adsorption capacities of the MB cation onto the different reported adsorbents

Materials	q_m (mg g^{-1})	Ref.
UiO-66/MIL-101(Fe)-GOCOOH	448.7	37
MIL-100 (Fe)	736.2	24
Ce(III)-doped UiO-66	145.3	40
Ce(III)-doped UiO-67	398.9	41
MIL-101-SO$_3$H	351.0	42
Amino-MIL-101(Al)	762.0	43
MOF-235	252.0	44
NH$_2$- MIL-125	405.6	44
Er-MOF	192.3	45
VNU-17	579.6	This work
VNU-23	**1992**	**This work**

capacity for MB (q_m = 1992 mg g^{-1}) as compared with the other adsorbents. The high adsorption capacity can be explained by the effective attraction interactions of SO$_3^-$ moieties inside VNU-23 with MB$^+$ cation. According to the obtained results, VNU-23 is chosen as an efficient and reusable adsorbent for removing cationic dyes from wastewater.

Plausible adsorption mechanism for VNU-23

The functional groups, the pore window/channel sizes, surface areas, and pore volumes of MOFs can influence the adsorption possibility of materials.[46] It is noted that the pore window and cage of VNU-23 are sufficient for MB to enter along the channels in the Oz axis (Fig. S1†). Based on the SO$_3$H groups existing within the structure of VNU-23, the adsorption mechanism of MB can be supposed to have several interactions, incorporating electrostatic interaction and π–π stacking. To demonstrate the mentioned hypothesis, we have performed a series of additional experiments. Firstly, the FT-IR spectra of MB⊂VNU-23 display unique peaks, centered at 1661 and 1333 cm^{-1}, that are absent in the spectrum of VNU-23. These are assigned to the $v_{C=N}$ and v_{C-N-C} vibrational modes of MB molecules, respectively (Fig. S7†). Notably, the peak at 1556 cm^{-1} for VNU-23 is attributed to the C=C vibrations in the benzene ring. However, for MB⊂VNU-23, this peak exhibits a difference from the peak at 1480 cm^{-1}. Such a change maybe from the π–π interactions between the channel wall and the conjugate planes of MB molecules.[47] Moreover, the two adsorption bands for MB⊂VNU-23 centered at 1135 and 1176 cm^{-1} correspond to the sulfonic groups' vibrational modes. These bands display a shift to the lower frequency in comparison with the original peaks of the sulfonic groups within VNU-23, which suggests that the mechanism of adsorption of MB onto VNU-23 includes electrostatic interactions between the SO$_3^-$ groups and MB$^+$. This is in good accordance with the previous report.[48]

To further confirm the stated interactions, the PXRD patterns of dyes⊂VNU-23 have been investigated. Recalling the evidence that the structural order of VNU-23 is lost after activation (see Fig. S9†), we expect that if the dye molecules are successfully diffused into the pores of VNU-23, its structure will be retained upon activation. Hence, PXRD analyses are conducted for the effective evaluation of whether the dye molecules

are loaded into the pores of VNU-23.[29,30] Consequently, as given in Fig. S10,† the PXRD pattern shows that MB⊂VNU-23 (absorbed at pH = 7) retains its crystallinity after activation, thus proving the diffusion of MB within the internal pores of VNU-23 via electrostatic and π–π interactions. Also, Rietveld refinement is carried out to match the simulated and experimental PXRD patterns of MB⊂VNU-23, to obtain a deeper insight into the loading of MB within the pores of VNU-23 (Fig. S11†).

To verify the specific π–π interactions inside the pores, VNU-23 is soaked in MB solution at pH = 3, which facilitates the formation of neutral MB molecules (pK_a = 3.8).[49] The PXRD analysis of activated MB⊂VNU-23 (absorbed at pH = 3) is in reasonable conformity with that of the simulated VNU-23, resulting in the conclusion that the neutral MB molecules are loaded into the channel wall of VNU-23 through π–π interactions (Fig. S10†). Similarly, rhodamine B (RhB$^+$, 6.8 × 11.8 × 15.8 Å), as a cationic dye, is loaded onto VNU-23 at pH = 7. The size of the RhB$^+$ molecules is unsuitable for entering the pores of VNU-23, driving to a poor adsorption capacity for RhB onto VNU-23 (ca. 42 mg g^{-1}), which is attributed to the adsorption of RhB onto the external surface of the framework. This results from the loss of structural order for the RhB⊂VNU-23 sample (Fig. S10†).

4. Conclusion

In summary, a series of experiments for the adsorption of MB onto Zr-sulfonic-based MOFs have been performed. It is noted that the maximum adsorption capacity for MB onto VNU-23 is found to be 1992 mg g^{-1} at pH = 7. This value is much higher than that of other MOFs and most the other porous materials reported previously. The equilibrium data are studied using the Langmuir, Freundlich, Temkin, and Dubinin–Radushkevich isotherm models. The results exhibit that the experimental data are efficiently correlated by the Langmuir adsorption isotherm. In addition, the kinetic mechanism is studied by using the pseudo first order, pseudo second order, and intra-particle diffusion models. The obtained results reveal a good agreement between the experimental data and the pseudo second order kinetic model. Here, the MB adsorption over VNU-23 can be explained to be through electrostatic attraction and π–π interactions. Furthermore, the recyclability tests indicate a good capability of reusing VNU-23 for many cycles with no significant reduction in the adsorption capacity, confirming the practical applications of our work.

Conflicts of interest

The authors maintain that they have no conflict of interest for this communication.

Acknowledgements

Notes and references

1 H. Xue, Q. Chen, F. Jiang, D. Yuan, G. Lv, L. Liang, L. Liu and M. Hong, A regenerative metal-organic framework for reversible uptake of Cd(ii): from effective adsorption to *in situ* detection, *Chem. Sci.*, 2016, **7**, 5983–5988.

2 M. T. Yagub, T. K. Sen, S. Afroze and H. M. Ang, Dye and its removal from aqueous solution by adsorption: a review, *Adv. Colloid Interface Sci.*, 2014, **209**, 172–184.

3 V. A. Shenai, Azo dyes on textile *vs*. German ban, An objective assessment, *Chem. Wkly.*, 1995, **12**, 33–34.

4 M. A. Ahsan, A. R. P. Santiago, M. F. Sanad, J. M. Weller, O. F. Delgado, L. A. Barrera, V. M. Rojas, B. A. Tenorio, C. K. Chan and J. C. Noveron, Tissue paper-derived porous carbon encapsulated transition metal nanoparticles as advanced non-precious catalysts: Carbon-shell influence on the electrocatalytic behaviour, *J. Colloid Interface Sci.*, 2021, **581**, 905–918.

5 M. A. Ahsan, A. R. P. Santiago, A. Rodriguez, V. M. Rojas, B. A. Tenorio, R. Bernal and J. C. Noverona, Biomass-derived ultrathin carbon-shell coated iron nanoparticles as high-performance tri-functional HER, ORR and Fenton-like catalysts, *J. Cleaner Prod.*, 2020, **275**, 124141.

6 M. A. Ahsan, A. R. P. Santiago, A. N. Nair, J. M. Weller, M. F. Sanad, D. J. V. Rosales, C. K. Chan, S. Sreenivasan and J. C. Noverona, Metal-organic frameworks-derived multifunctional carbon encapsulated metallic nanocatalysts for catalytic peroxymonosulfate activation and electrochemical hydrogen generation, *Mol. Catal.*, 2020, **498**, 111241.

7 S. Wu, Y. Lin, C. Yang, C. Du, Q. Teng, Y. Ma, D. Zhang, L. Nie and Y. Zhong, Enhanced activation of peroxymonosulfte by LaFeO$_3$ perovskite supported on Al$_2$O$_3$ for degradation of organic pollutants, *Chemosphere*, 2019, **237**, 124478.

8 K. Guo, B. Gao, X. Tian, Q. Yue, P. Zhang, X. Shen and X. Xu, Synthesis of polyaluminium chloride/papermaking sludge-based organic polymer composites for removal of disperse yellow and reactive blue by flocculation, *Chemosphere*, 2019, **231**, 337–348.

9 G. Yang, D. Zhang, G. Zhu, T. Zhou, M. Song, L. Qu, K. Xiong and H. Li, A Sm-MOF/GO nanocomposite membrane for efficient organic dye removal from wastewater, *RSC Adv.*, 2020, **10**, 8540–8547.

10 D. Bassyouni, H. Hamad, E. Z. El-Ashtoukhy, N. Amin and M. A. El-Latif, Comparative performance of anodic oxidation and electrocoagulation as clean processes for electrocatalytic degradation of diazo dye Acid Brown 14 in aqueous medium, *J. Hazard. Mater.*, 2017, **335**, 178–187.

11 A. Dey, S. K. Konavarapu, H. S. Sasmal and K. Biradha, Porous Coordination Polymers Containing Pyridine-3,5-Bis(5-azabenzimidazole): Exploration of Water Sorption, Selective Dye Adsorption, and Luminescent Properties, *Cryst. Growth Des.*, 2016, **16**, 5976–5984.

12 A. E. Burakov, E. V. Galunin, I. V. Burakova, A. E. Kucherova, S. Agarwal, A. G. Tkachev and V. K. Gupta, Adsorption of heavy metals on conventional and nanostructured materials for wastewater treatment purposes: A review, *Ecotoxicol. Environ. Saf.*, 2018, **148**, 702–712.

13 X. Inthapanya, S. Wu, Z. Han, G. Zeng, M. Wu and C. Yang, Adsorptive removal of anionic dye using calcined oyster shells: isotherms, kinetics, and thermodynamics, *Environ. Sci. Pollut. Res.*, 2019, **26**, 5944–5954.

14 M. Elkady, H. Shokry, A. El-Sharkawy, G. El-Subruiti and H. Hamad, New insights into the activity of green supported nanoscale zero-valent iron composites for enhanced acid Blue-25 dye synergistic decolorization from aqueous medium, *J. Mol. Liq.*, 2019, **294**, 111628.

15 N. Wang, Y. F. Wang, A. M. Omer and X. K. Ouyang, Fabrication of novel surface-imprinted magnetic graphene oxide-grafted cellulose nanocrystals for selective extraction and fast adsorption of fluoroquinolones from water, *Anal. Bioanal. Chem.*, 2017, **409**, 6643–6653.

16 T. M. Tamer, W. M. Abou-Taleb, G. D. Roston, M. S. Mohyeldin, A. M. Omer, R. E. Khalifa and A. M. Hafez, Formation of zinc oxide nanoparticles using alginate as a template for purification of wastewater, *Environ. Nanotechnol. Monit. Manag.*, 2018, **10**, 112–121.

17 A. W. Tan, B. H. Hameed and A. L. Ahmad, Equilibrium and kinetic studies on basic dye adsorption by oil palm fibre activated carbon, *Chem. Eng. J.*, 2007, **127**, 111–119.

18 A. M. M. Vargas, A. L. Cazetta, M. H. Kunita, T. L. Silva and V. C. Almeida, Adsorption of methylene blue on activated carbon produced from flamboyant pods (Delonix regia): Study of adsorption isotherms and kinetic models, *Chem. Eng. J.*, 2011, **168**, 722–730.

19 Z. Zhang and J. Kong, Novel magnetic Fe$_3$O$_4$@C nanoparticles as adsorbents for removal of organic dyes from aqueous solution, *J. Hazard. Mater.*, 2011, **193**, 325–329.

20 W. Cheung, Y. Szeto and G. McKay, Intraparticle diffusion processes during acid dye adsorption onto chitosan, *Bioresour. Technol.*, 2007, **98**, 2897–2904.

21 F. M. Machado, S. A. Carmalin, E. C. Lima, S. L. P. Dias, L. D. T. Prola, C. Saucier, I. M. Jauris, I. Zanella and S. B. Fagan, Adsorption of Alizarin Red S Dye by Carbon Nanotubes: An Experimental and Theoretical Investigation, *J. Phys. Chem. C*, 2016, **120**, 18296–18306.

22 H. Furukawa, K. E. Cordova, M. O'Keeffe and O. M. Yaghi, The chemistry and applications of metal-organic frameworks, *Science*, 2013, **341**, 1230444.

23 E. Haque, J. W. Jun and S. H. Jhung, Adsorptive removal of methyl orange and methylene blue from aqueous solution with a metal-organic framework material, iron terephthalate (MOF-235), *J. Hazard. Mater.*, 2011, **185**, 507–511.

24 M. Tong, D. Liu, Q. Yang, S. D. Vinot, G. Maurin and C. Zhong, Influence of framework metal ions on the dye capture behaviour of MIL-100 (Fe, Cr) MOF type solids, *J. Mater. Chem. A*, 2013, **1**, 8534–8537.

25 Z. P. Qi, J. M. Yang, Y. S. Kang, F. Guo and W. Y. Sun, Facile water-stability evaluation of metal–organic frameworks and the property of selective removal of dyes from aqueous solution, *Dalton Trans.*, 2016, **45**, 8753–8759.

26 H. Xue, X. Huang, Q. Yin, X. Hu, H. Zheng, G. Huang and T. Liu, Bimetallic cationic metal–organic frameworks for selective dye adsorption and effective $Cr_2O_7^{2-}$ removal, *Cryst. Growth Des.*, 2020, **20**, 4861–4866.

27 M. Guo, H. Guo, S. Liu, Y. Suna and X. Guo, A microporous cationic metal–organic framework for the efficient removal of dichromate and the selective adsorption of dyes from water, *RSC Adv.*, 2017, **7**, 51021–51026.

28 H. Li, X. Cao, C. Zhang, Q. Yu, Z. Zhao, X. Niu, X. Sun, Y. Liu, L. Ma and Z. Li, Enhanced adsorptive removal of anionic and cationic dyes from single or mixed dye solutions using MOF PCN-222, *RSC Adv.*, 2017, **7**, 16273–16281.

29 T. H. N. Lo, M. V. Nguyen and T. N. Tu, An anchoring strategy leads to enhanced proton conductivity in a new metal-organic framework, *Inorg. Chem. Front.*, 2017, **4**, 1509–1516.

30 M. V. Nguyen, T. H. N. Lo, L. C. Luu, H. T. T. Nguyen and T. N. Tu, Enhancing proton conductivity in a metal-organic framework at $T > 80\ °C$ by an anchoring strategy, *J. Mater. Chem. A*, 2018, **6**, 1816–1821.

31 V. Bon, I. Senkovska, M. S. Weissb and S. Kaskela, Tailoring of network dimensionality and porosity adjustment in Zr- and Hf-based MOFs, *CrystEngComm*, 2013, **15**, 9572–9577.

32 F. Yang, H. Huang, X. Wang, F. Li, Y. Gong, C. Zhong and J. Li, Proton conductivities in functionalized UiO-66: tuned properties, thermogravimetry mass, and molecular simulation analyses, *Cryst. Growth Des.*, 2015, **15**, 5827–5833.

33 F. Yang, G. Xu, Y. Dou, B. Wang, H. Zhang, H. Wu, W. Zhou, J. Li and B. Chen, A flexible metal-organic framework with a high density of sulfonic acid sites for proton conduction, *Nat. Energy*, 2017, **2**, 877–883.

34 E. M. El-Sayed, T. M Tamer, A. M. Omer and M. S. M. Eldin, Development of novel chitosan Schiff base derivatives for cationic dye removal: methyl orange model, *Desalin. Water Treat.*, 2016, **57**, 22632–22645.

35 A. G. El-Shamy and H. S. S. Zayied, New polyvinyl alcohol/carbon quantum dots (PVA/CQDs) nanocomposite films: structural, optical and catalysis properties, *Synth. Met.*, 2020, **259**, 116218.

36 H. Dai, Y. Huang and H. Huang, Eco-friendly polyvinyl alcohol/carboxymethyl cellulose hydrogels reinforced with graphene oxide and bentonite for enhanced adsorption of methylene blue, *Carbohydr. Polym.*, 2018, **185**, 1–11.

37 A. S. Eltaweil, E. M. A. El-Monaem, G. M. El-Subruiti, M. M. A. El-Latifb and A. M. Omer, Fabrication of UiO-66/MIL-101(Fe) binary MOF/carboxylated-GO composite for adsorptive removal of methylene blue dye from aqueous solutions, *RSC Adv.*, 2020, **10**, 19008–19019.

38 A. M. Omer, R. E. Khalifa, T. Tamer, M. Elnouby, A. Hamed, Y. Ammar, A. Ali, M. Gouda and M. M. Eldin, Fabrication of a novel low-cost superoleophilic nonanyl chitosan-poly (butyl acrylate) grafted copolymer for the adsorptive removal of crude oil spills, *Int. J. Biol. Macromol.*, 2019, **140**, 588–599.

39 A. M. Omer, R. E. Khalifa, Z. Hu, H. Zhang, C. Liu and X. K. Ouyang, Fabrication of tetraethylenepentamine functionalized alginate beads for adsorptive removal of Cr(vi) from aqueous solutions, *Int. J. Biol. Macromol.*, 2019, **125**, 1221–1231.

40 J. M. Yang, R. J. Ying, C. X. Han, Q. T. Hu, H. M. Xu, J. H. Li, Q. Wang and W. Zhang, Adsorptive removal of organic dyes from aqueous solution by a Zr-based metal-organic framework: effects of Ce(iii) doping, *Dalton Trans.*, 2018, **47**, 3913–3920.

41 J. M. Yang, B. C. Yang, Y. Zhang, R. N. Yang, S. S. Ji, Q. Wang, S. Quan and R. Z. Zhang, Rapid adsorptive removal of cationic and anionic dyes from aqueous solution by a Ce(iii)-doped Zr-based metal-organic framework, *Microporous Mesoporous Mater.*, 2020, **292**, 109764–110970.

42 X. P. Luo, S. Y. Fu, Y. M. Du, J. Z. Guo and B. Li, Adsorption of methylene blue and malachite green from aqueous solution by sulfonic acid group modified MIL-101, *Microporous Mesoporous Mater.*, 2017, **237**, 268–274.

43 E. Haque, V. Lo, A. I. Minett, A. T. Harris and T. L. Church, Dichotomous adsorption behaviour of dyes on an amino-functionalised metal-organic framework, amino-MIL-101(Al), *J. Mater. Chem. A*, 2014, **2**, 193–203.

44 R. Bibi, L. Wei, Q. Shen, W. Tian, O. Oderinde, N. Li and J. Zhou, Effect of amino functionality on the uptake of cationic dye by Titanium-based metal organic frameworks, *J. Chem. Eng. Data*, 2017, **62**, 1615–1622.

45 M. Mohammadnejad, T. Hajiashra and R. Rashnavadi, An erbium-organic framework as an adsorbent for the fast and selective adsorption of methylene blue from aqueous solutions, *J. Porous Mater.*, 2018, **25**, 761–769.

46 Z. J. Lin, H. Q. Zheng, H. Y. Zheng, L. P. Lin, Q. Xin and R. Cao, Efficient capture and effective sensing of $Cr_2O_7^{2-}$ from water using a zirconium metal-organic framework, *Inorg. Chem.*, 2017, **56**, 14178–14188.

47 S. Q. Deng, Y. L. Miao, Y. L. Tan, H. N. Fang, Y. T. Li, X. J. Mo, S. L. Cai, J. Fan, W. G. Zhang and S. R. Zheng, An anionic nanotubular metal-organic framework for high capacity dye adsorption and dye degradation in darkness, *Inorg. Chem.*, 2019, **58**, 13979–13987.

48 G. Vijayakumar, R. Tamilarasan and M. Dharmendirakumar, Adsorption, Kinetic, Equilibrium and thermodynamic studies on the removal of basic dye Rhodamine-B from aqueous solution by the use of natural adsorbent perlite, *J. Mater. Environ. Sci.*, 2012, **3**, 157–170.

49 O. S. Bayomie, H. Kandeel, T. Shoeib, H. Yang, N. Youssef and M. M. H. El-Sayed, Novel approach for effective removal of methylene blue dye from water using bean peel waste, *Sci. Rep.*, 2020, **10**, 7824.